Author's preprint
Published as J. Chem. Phys. **146**, 134310 (2017)

Crossing the dividing surface of transition state theory. IV. Dynamical regularity and dimensionality reduction as key features of reactive trajectories

J. C. Lorquet[a)]

Department of Chemistry, University of Liège, Sart-Tilman (Bâtiment B6), B-4000 Liège 1, Belgium

[a)] Electronic mail: jc.lorquet@ulg.ac.be

ABSTRACT

The atom-diatom interaction is studied by classical mechanics using Jacobi coordinates (R, r, θ). Reactivity criteria that go beyond the simple requirement of transition state theory (i.e., $P_{R^*} > 0$) are derived in terms of specific initial conditions. Trajectories that exactly fulfill these conditions cross the conventional dividing surface used in transition state theory (i.e., the plane in configuration space passing through a saddle point of the potential energy surface and perpendicular to the reaction coordinate) only once. Furthermore, they are observed to be strikingly similar and to form a tightly-packed bundle of perfectly collimated trajectories in the two-dimensional (R, r) configuration space, although their angular motion is highly specific for each one. Particular attention is paid to symmetrical transition states (i.e., either collinear or T-shaped with C_{2v} symmetry) for which decoupling between angular and radial coordinates is observed, as a result of selection rules that reduce to zero Coriolis couplings between modes that belong to different irreducible representations. Liapunov exponents are equal to zero and Hamilton's characteristic function is planar in that part of configuration space that is visited by reactive trajectories. Detailed consideration is given to the concept of average reactive trajectory, which starts right from the saddle point and which is shown to be free of curvature-induced Coriolis coupling. The reaction path Hamiltonian model, together with a symmetry-based separation of the angular degree of freedom, provide an appropriate framework that leads to the formulation of an effective two-dimensional Hamiltonian. The success of the adiabatic approximation in this model is due to the symmetry of the transition state, not to a separation of time scales. Adjacent trajectories, i.e., those that do not exactly fulfill the reactivity conditions have similar characteristics, but the quality of the approximation is lower. At higher energies, these characteristics persist, but to a lesser degree. Recrossings of the dividing surface then become much more frequent and the phase space volume of initial conditions that generate recrossing-free trajectories decreases. Altogether, one ends up with an additional illustration of the concept of reactive cylinder (or conduit) in phase space that reactive trajectories must follow. Reactivity is associated with dynamical regularity and dimensionality reduction, whatever the shape of the potential energy surface, no matter how strong its anharmonicity, and whatever the curvature of its reaction path. Both simplifying features persist during the entire reactive process, up to complete separation of fragments. The ergodicity assumption commonly assumed in statistical theories is inappropriate for reactive trajectories.

I. INTRODUCTION

In transition state theory (TST), a crucial issue relates to the separability of the reaction coordinate.[1] As early as 1939, Hirschfelder and Wigner[2] drew attention to the great simplification that can be achieved by making use of the principle of adiabatic invariance to separate the slow motion in the reaction coordinate from the bath of other motions. Marcus[3,4] and Truhlar[5] then expanded on this idea.

A decisive point was reached when Miller pointed out that conserved action variables exist in the neighborhood of the saddle point of a potential energy surface, even in the nonseparable case[6-8]. Together with his co-workers, he developed the idea that in the saddle point region the imaginary action variable cannot be coupled to the real actions of the other degrees of freedom.

More recently, additional arguments in favor of the existence of approximate invariants of motion in the neighborhood of a first-order saddle point have been put forward.

Theoretical studies on isomerization reactions of atomic clusters by Berry and co-workers showed a decrease of local Liapunov exponents in the regions of saddles compared with those in the potential well[9-12]. Classical trajectory calculations revealed the existence of regularities in the motion near the saddle in the form of a "collimation" of trajectories. These authors invested considerable effort in the search for recrossing-free dividing surfaces in phase space by using a perturbation theory to transform the system of coordinates so as to make the new Hamiltonian as close to integrable as possible.[12]

Mathematically rigorous foundations were laid by Wiggins and co-workers[13-15] for the understanding of local regularities in the dynamics of a classical motion in the neighborhood of a saddle point. These authors used a system of so-called normal form coordinates, mixing coordinates and momenta, to decouple the Hamiltonian. The analysis is completely general and locally conserved action variables were shown to exist even when the Hamiltonian is highly dimensional and involves a non-separable anharmonic potential energy function.

The present contribution is the fourth in a series devoted to the study of classical motion in the neighborhood of a saddle point. In papers I and II,[16, 17] evidence was given for the existence of symmetries, in the form of motion coordination among a bundle of trajectories crossing the saddle point region. In paper III,[18] instead of trying to determine a recrossing-free dividing surface in phase space, we looked for a way to select trajectories that do not recross the conventional surface in configuration space. This means that the plane containing

the saddle point and perpendicular to the unstable vibrational mode is no longer seen as a dividing surface separating reactants and products: instead, it serves to define initial conditions that generate truly reactive trajectories. This enabled us to put forward a method for choosing initial conditions capable of generating reactive trajectories.

We wish to go further in the present contribution. In Sec. II, we focus on the particular case of symmetrical TSs (i.e., either collinear or C_{2v} T-shaped) and seek to identify those properties that characterize reactive trajectories irrespective of the expression of the potential energy surface: decoupling and dimensionality reduction are among them. In Sec. III, we consider a specific Hamiltonian and recapitulate briefly the main results derived in paper III, putting the reactivity criteria valid for symmetrical TSs in concrete form. An application to the formyl radical decomposition is presented in Sec. IV, for which reactive loci in phase space are determined. In Sec. V, reactive trajectories are shown to be surprisingly similar; they are characterized by a decoupling of the angular degree of freedom and by a grouping property in the two-dimensional *(R, r)* subspace. The decoupling properties established in this way suggest that it should be possible to derive an effective 2D Hamiltonian, which is done in Sec. VI. A proper framework to analyze these results is shown in Sec. VII to be based on the reaction path Hamiltonian model. The striking grouping of reactive trajectories is discussed in Sec. VIII. The robustness of our results is checked by considering the influence of an increase of the internal energy in Sec. IX. The case of T-shaped TSs is briefly considered in Sec. X. Sec. XI concludes.

II. GENERAL FEATURES OF REACTIVE TRAJECTORIES

A. Analytical equations of motion

As shown in detail by Hirschfelder,[19] it is possible to derive a system of coordinates, valid for any polyatomic molecule, where the reaction coordinate is separable over its entire range, by defining it as the distance between the centers of mass of the two separating fragments. However, the remaining coordinates that represent the vibrational motion inside each fragment are then extremely complicated and unphysical. Fortunately, the problem does not arise in the particular case of a triatomic system studied in a body-fixed rotationless frame. The kinetic energy can be written quite simply in Jacobi coordinates and remains valid at all internuclear distances. The following Hamiltonian[13, 16-18] thus conveniently describes the atom-diatom interaction

$$H = \frac{P_R^2}{2M} + \frac{P_r^2}{2\mu} + \frac{1}{2}\left(\frac{1}{MR^2} + \frac{1}{\mu r^2}\right)P_\theta^2 + V(R,r,\theta) \qquad (2.1)$$

where R is the distance between the atom and the center of mass of the diatomic, r the internuclear distance of the latter, θ the angle between the two position vectors, P_R, P_r, P_θ the conjugate momenta, μ the reduced mass of the diatomic, and M that of the atom - diatom system. The potential energy function is so far completely arbitrary, except that it is characterized by a saddle point at coordinates (R_*, r_*, θ_*).

In paper III[18] we put forward a method for choosing initial conditions that generate reactive trajectories, and that is valid for a very general shape of potential energy surfaces, characterized only by the presence of a first-order saddle point. (Such complications as non-minimum energy path reactions,[20] valley-ridge inflection points,[21, 22] roaming,[23, 24] etc., are excluded.) The method is based on a general procedure to derive analytic equations of motion by repeated applications of the Poisson bracket equation.[25] The equation of motion of any dynamical variable X, coordinate or momentum, can be obtained as a series expansion

$$X(t) = X_0 + t[X,H]_0 + \frac{t^2}{2!}[[X,H],H]_0 + \ldots \qquad (2.2)$$

where the subscript zero refers to the initial conditions at time $t = 0$.

Of particular interest is the case $X = R$, where R is the translational coordinate. Its equation of motion can be formulated as follows:

$$R(t) = R_* + \frac{P_{R*}}{M}t + c_2\left(\frac{t^2}{2!}\right) + c_3\left(\frac{t^3}{3!}\right) + \ldots \qquad (2.3)$$

where R_* denotes the position of the saddle point, reached at $t = 0$.

In conventional TST, the condition $P_{R*} > 0$ is the only prerequisite for a classical trajectory to be deemed reactive. However, as explained in detail in Paper III,[18] additional restrictions should be introduced. A trajectory will be reactive if its initial conditions are chosen so that

1) even-power coefficients (quadratic, quartic, ...) are absent from the Taylor expansion of the actual equation of motion (i.e., from Eq. (2.3)) because these terms inflect the trajectory and induce recrossings at positive times (if $c_2 < 0$) or at negative times (if $c_2 > 0$).

2) odd-power coefficients (linear, cubic, quintic, ...) are all positive (and as large as possible).

B. A general Hamiltonian describing symmetrical TSs

Let us now go back to the general expression of the Hamiltonian written in Jacobi coordinates (Eq. (2.1)). Given the experience acquired in Paper III, we know that the algebra becomes much simpler when the TS is collinear. Simplifications also arise if it has C_{2v} symmetry in its equilibrium conformation, i.e., if it is T-shaped, with an equilibrium bending angle equal to $\pi/2$ and if the diatomic moiety is homonuclear.

We return to Eqs. (2.2) and (2.3) with the aim of finding general properties of reactive trajectories when the expression of the potential function V is left unspecified, except that $V(R_*, r, \theta)$ is required to be an even function of θ (for a collinear TS) or of $(\theta - \pi/2)$ (if the TS has C_{2v} symmetry at its stationary point).

In the particular case of a collinear TS, the set of initial conditions is denoted as $\left\{R_*, P_{R_*}, r_* + \delta r, p_r, \delta\theta, p_\theta\right\}$. For a C_{2v} T-shaped TS, the set would be $\left\{R_*, P_{R_*}, r_* + \delta r, p_r, \frac{\pi}{2} + \delta\theta, p_\theta\right\}$. (To alleviate the notation, the initial conditions δr, $\delta\theta$, p_r, and p_θ are written in lower case letters without any asterisk.) The coefficient in Eq. (2.3) that controls reactivity is

$$c_2 = \left[\left[R,H\right],H\right]_0 = \frac{p_\theta^2}{M^2 R_*^3} - \frac{1}{M}\left.\frac{\partial V}{\partial R}\right|_0 , \tag{2.4}$$

where the asterisk denotes the coordinates $(R_*, r_*, 0)$ or $(R_*, r_*, \pi/2)$ of the saddle point. The solution of the equation $c_2 = 0$ gives the appropriate value to be given to the initial elongation δr in order to have a reactive trajectory. One gets

$$\delta r = \left(\left.\frac{\partial^2 V}{\partial R\,\partial r}\right|_*\right)^{-1}\left(\frac{p_\theta^2}{M R_*^3} - \frac{1}{2}\left.\frac{\partial^3 V}{\partial R\,\partial\theta^2}\right|_* \delta\theta^2\right). \tag{2.5}$$

This particular choice of initial conditions plays an essential role in all of the developments that follow. We submit that it is one of the key concepts in the rationalization of reactivity.

The next requirement is that the cubic coefficient c_3 should be positive and as large as possible. The corresponding nested expression in Eq. (2.2) has been evaluated for a general potential V at the particular value of δr formulated in Eq. (2.5) and then expanded in a Taylor series in $\delta\theta$ and p_θ. One gets

$$c_3 = -\frac{P_{R*}}{M^2}\left.\frac{\partial^2 V}{\partial R^2}\right|_* - \frac{p_r}{M\mu}\left.\frac{\partial^2 V}{\partial R\,\partial r}\right|_* - \left(2\frac{1}{M^2 R_*^3}\left.\frac{\partial^2 V}{\partial \theta^2}\right|_* + \frac{1}{M I_*}\left.\frac{\partial^3 V}{\partial R\,\partial \theta^2}\right|_*\right)\delta\theta\, p_\theta + \ldots \qquad (2.6)$$

The first term of this expression is necessarily positive, whereas the appropriate sign to be given to the vibrational momentum p_r to promote reactivity should be coordinated with that of a cross-term in the expansion of the potential energy surface, i.e.,

$$p_r \left.\frac{\partial^2 V}{\partial R\,\partial r}\right|_* < 0\,. \qquad (2.7)$$

The third term plays a minor role, as will become clear later on.

Similar calculations were done for the next higher coefficients. For the quintic coefficient, one finds

$$c_5 = \frac{P_{R*}}{M^2}\left(\frac{1}{M}\left(\left.\frac{\partial^2 V}{\partial R^2}\right|_*\right)^2 + \frac{1}{\mu}\left(\left.\frac{\partial^2 V}{\partial R\,\partial r}\right|_*\right)^2\right) + \frac{p_r}{M\mu}\left.\frac{\partial^2 V}{\partial R\,\partial r}\right|_*\left(\frac{1}{M}\left.\frac{\partial^2 V}{\partial R^2}\right|_* + \frac{1}{\mu}\left.\frac{\partial^2 V}{\partial r^2}\right|_*\right) + \ldots \qquad (2.8)$$

to which numerous terms involving the product $\delta\theta\, p_\theta$ should be added. Note that the coefficient of P_{R*} is a sum of squares and therefore always positive whereas the sign of the initial vibrational momentum should again be chosen appropriately to make sure that it promotes reactivity.

Even-order coefficients have a reduced influence because of the heaviness of the nuclear masses: k-th order terms in Eq. (2.3) are proportional to $M^{-(k+1)/2}$ if k is odd and to $M^{-(k+2)/2}$ if k is even.[18]

Unfortunately, the complexity of the coefficients c_j that appear in Eq. (2.3) increases very rapidly with their order. This limits the applicability of the analytical approach to a certain range on either side of the dividing surface. However, as it turns out, this range is broad enough to derive useful information on the dynamics.

C. Dynamical reaction path and average reactive trajectory

Several groups have long observed that reactive trajectories get together in the form of reactive "tubes" or "cylinders" or "conduits" in phase space.[13-15, 26-28] Calculations done by Fair *et al.*[27] and by Waalkens *et al.*[13] offer spectacular illustrations of these structures. The center line of these cylinders has been termed the dynamical reaction path.[13-15] This

grouping implies that graphs representing the motion along the reaction coordinate (i.e., plots of *R(t)*) can be expected to look roughly the same for reactive, non-recrossing trajectories. It makes therefore sense in the present study to average Eq. (2.3) over sets of four initial conditions ($\pm \delta\theta, \pm p_\theta$) because, for symmetrical TSs, these four states have the same energy. This procedure eliminates many terms and leads to a simple expression of the average equation of motion of reactive trajectories that depends on P_{R*} and p_r alone and in which all reference to $\delta\theta$ and p_θ disappears. If the initial conditions satisfy Eq. (2.5) one obtains

$$\langle R(t)\rangle = R_* + \frac{P_{R*}}{M}\,t + \langle c_3\rangle\left(\frac{t^3}{3!}\right) + \langle c_5\rangle\left(\frac{t^5}{5!}\right) + \ldots \tag{2.9}$$

where $\langle c_3\rangle$ and $\langle c_5\rangle$ are equal to the sum of the first two terms reported in Eqs. (2.6) and (2.8), respectively.

The same procedure can used to derive the expression of the average equation of motion of the vibrational coordinate for reactive trajectories. One gets

$$\langle r(t)\rangle = r_* + \frac{p_r}{\mu}\,t + \langle a_3\rangle\left(\frac{t^3}{3!}\right) + \langle a_5\rangle\left(\frac{t^5}{5!}\right) + \ldots \tag{2.10}$$

where

$$\langle a_3\rangle = -\frac{p_r}{\mu^2}\left.\frac{\partial^2 V}{\partial r^2}\right|_* - \left.\frac{P_{R*}}{M\,\mu}\frac{\partial^2 V}{\partial R\,\partial r}\right|_* \tag{2.11}$$

$$\langle a_5\rangle = \frac{p_r}{\mu^2}\left(\frac{1}{\mu}\left(\left.\frac{\partial^2 V}{\partial r^2}\right|_*\right)^2 + \frac{1}{M}\left(\left.\frac{\partial^2 V}{\partial R\,\partial r}\right|_*\right)^2\right) + \left.\frac{P_{R*}}{M\,\mu}\;\frac{\partial^2 V}{\partial R\,\partial r}\right|_*\left(\frac{1}{\mu}\left.\frac{\partial^2 V}{\partial r^2}\right|_* + \frac{1}{M}\left.\frac{\partial^2 V}{\partial R^2}\right|_*\right). \tag{2.12}$$

Here again, the average equation of motion of the vibrational coordinate for reactive trajectories is found to depend on p_r and P_{R*} alone, which therefore should be considered as essential parameters in the equations of motion of a reactive trajectory.

Finally, due to the assumed symmetry of the TS, one finds $\langle\theta(t)\rangle = 0$.

In summary, irrespective of the shape of the potential energy surface (except for the fact that the TS is assumed to be symmetrical), the bundle of reactive trajectories obeying the zero-initial acceleration condition $c_2 = 0$ is seen to be grouped around an average trajectory that is determined by the two initial conditions P_{R*} and p_r only. Any energy deposited as translational momentum P_{R*} necessarily stimulates reactivity, as intuitively expected. Energy delivered as vibrational momentum can be beneficial if the inequality (2.7) is fulfilled, but

curbs reactivity otherwise. Energy deposited in the angular motion is less effective and is responsible for the dispersion of individual trajectories.

D. A reduced-dimensionality effective Hamiltonian for symmetrical TSs

The fact that the angular variables θ and p_θ do not appear in the average equation of motion of the translational and vibrational degrees of freedom suggests that it should be possible to reduce the dimensionality of the problem. The possibility should exist to calculate the laws of motion of the average reactive trajectory of a symmetrical TS for the *R* and *r* degrees of freedom by applying Hamilton's equations of motion to an effective two-dimensional Hamiltonian

$$H_{2D} = \frac{P_R^2}{2M} + \frac{P_r^2}{2\mu} + V_{2D}(R, r) \qquad (2.13)$$

where the potential V_{2D} is as yet unknown, except that it must be characterized by a symmetrical saddle point at coordinates (R_*, r_*).

Consider the particular trajectory that starts right at the saddle point, i.e., that has $\{R_*, P_{R_*}, r_*, p_r\}$ as initial conditions, and calculate its equations of motion via Eq. (2.2) without specifying the expression of the potential V_{2D}. It turns out that they reduce to Eqs. (2.9) and (2.10), with coefficients that are exactly equal to the average values $\langle c_3 \rangle$, $\langle c_5 \rangle$, $\langle a_3 \rangle$, and $\langle a_5 \rangle$ derived in the previous paragraph for the 3D Hamiltonian. This is also the case for the coefficients $\langle c_7 \rangle$ and $\langle a_7 \rangle$, which are not reported here because of the unwieldiness of their expression.

Since the eight average coefficients, from $\langle c_1 \rangle$ to $\langle c_7 \rangle$ and from $\langle a_1 \rangle$ to $\langle a_7 \rangle$, which appear in the average equations of motion of reactive trajectories for a 3D Hamiltonian depend on three quantities only (namely, $\partial^2 V/\partial R^2\big|_*$, $\partial^2 V/\partial R\,\partial r\big|_*$, and $\partial^2 V/\partial r^2\big|_*$), it follows that the constraints to be imposed on the construction of V_{2D} do not go beyond the requirement that these three second derivatives should be equal to those that characterize the actual three-dimensional potential.

When these three conditions are fulfilled, the equations of motion of the average reactive trajectory can be derived from the reduced-dimensionality effective Hamiltonian expressed in Eq. (2.13). It is important to note that the dimensionality reduction is valid for reactive trajectories only, i.e., when the initial conditions satisfy Eq. (2.5).

E. Synopsis

The scope of the treatment is limited to the dissociation of a triatomic molecule. In full conformity with the textbook paradigm, non-minimum energy paths,[20] bifurcations,[21, 22] and roaming[23, 24] are excluded. The TS is assumed to belong to $C_{\infty v}$ or C_{2v} point groups. No other assumption is made on the shape of the potential energy surface. The equations of motion are calculated as a series expansion. Analytical expressions of the coefficients are given, but up to the seventh order only. As a result of the unavoidable truncation of the series, these analytical equations of motion are valid over a restricted time range only. However, there is in principle no limitation if the series is calculated numerically.

Particular attention is paid to the subset that exactly fulfills Eq. (2.5), which will henceforth be referred to as the subset of central reactive trajectories. (The latter term was used in Paper III[18] in a more restricted sense, which we now wish to abandon.) They form a bundle that is expected to be grouped around its average. The equation of the average motion depends on two variables only, namely p_r and P_{R*}, without any reference to the angular mode, no matter how strong the anharmonicity of the potential energy surface, and whatever the curvature of its reaction path. Alternatively, it can be calculated quite simply from an equivalent two-dimensional Hamiltonian, either analytically over a restricted time range, or numerically up to complete separation of fragments.

This decoupling and the associated dimensionality reduction form the starting point and the leitmotiv of the present paper. However, several questions remain open. How tight is the bundle of reactive trajectories? How broad is the time range of validity? Can one be more specific about the decoupling mechanism? To answer these questions and to put the previous general results in concrete form, more information is needed about the shape of the Hamiltonian. A specific choice is studied in the next sections.

III. A SPECIFIC HAMILTONIAN FOR COLLINEAR TRANSITION STATES

In order to derive explicit reactivity criteria, the previous analysis was applied to a specific Hamiltonian designed to represent a typical potential energy surface presenting a saddle point of a type frequently encountered in molecular reaction dynamics. A collinear geometry is assumed. Since an in-depth presentation would be lengthy, we refer the reader to Papers II and III where full details are given[17, 18] and recapitulate only the essential features of the chosen model.

A. The model

The potential is written as a sum of two- and three-body contributions,

$$V(R, r, \theta) = V_{saddle}(R) + V_{diat}(r, R) + V_{ang}(\theta, R) + V_{3b}(R, r, \theta) . \quad (3.1)$$

The first term of this expansion, representing a cross-section along the reaction coordinate, is written as an inverted 6–12 Lennard-Jones potential where the zero of energy has been shifted to the saddle point.

$$V_{saddle}(R) = -\frac{M R_*^2 \Omega^2}{72}\left(1-\left(\frac{R_*}{R}\right)^6\right)^2 \quad (3.2)$$

where Ω denotes the modulus of an imaginary frequency which, as will be seen shortly (in Eq. (3.10)), is not an observable but a zeroth-order quantity.

The next two-body term describes the vibrational motion of the diatomic fragment. Since the present study aims at investigating decoupling among degrees of freedom, it seemed to us essential to take anharmonicity into account. To do this in a simple way, a Simons-Parr-Finlan potential is used.[29] Furthermore, curvature of the reaction path is introduced by allowing the frequency and equilibrium distance of the diatomic fragment to depend on the reaction coordinate R. Altogether,

$$V_{diat}(r,R) = \frac{1}{2}\mu\omega(R)^2\left(r - r_{eq}(R)\right)^2\left(\frac{r_{eq}(R)}{r}\right)^2 , \quad (3.3)$$

with

$$r_{eq}(R) = r_\infty + \left(r_* - r_\infty\right)\left(\frac{R_*}{R}\right)^6 , \quad (3.4)$$

$$\omega(R) = \omega_\infty + \left(\omega_* - \omega_\infty\right)\left(\frac{R_*}{R}\right)^6 , \quad (3.5)$$

where r_∞ and ω_∞ denote the equilibrium distance and angular frequency of the diatomic fragment after complete separation, respectively. The inverse sixth power dependence is in line with the assumption of an inverse Lennard-Jones potential for the reaction coordinate.

The potential that determines the angular motion, which is a hindered rotation with a strongly R-dependent barrier, is written as

$$V_{ang}(\theta,R) = V_0\left(\frac{R_*}{R}\right)^6 \sin^2\theta . \quad (3.6)$$

To derive the expression of the three-body interaction term, we adapt Murrell's procedure[30] to a saddle point topography described in Jacobi coordinates. As described in detail in Paper II,[17] we write

$$V_{3b}(R,r,\theta) = P_{3b}(R,r,\theta)\left(\frac{R_*}{R}\right)^6\left(1-\left(\frac{R_*}{R}\right)^6\right)\left(1-\tanh\left(\frac{\gamma}{2}\left(r-r_{eq}(R)\right)\right)\right), \tag{3.7}$$

with, in the case of a collinear TS,

$$P_{3b}(R,r,\theta) = \beta_{RR}\left(R-R_*\right)^2 + \beta_{rr}\left(r-r_*\right)^2 + \beta_{\theta\theta}\,\theta^2 + \beta_{Rr}\left(R-R_*\right)\left(r-r_*\right). \tag{3.8}$$

The second-order expansion of the whole potential energy surface about the saddle point is

$$V\left(R,r,\theta\right) = -\frac{1}{2}k_{saddle}\left(R-R_*\right)^2 + \frac{1}{2}\mu\omega_*^2\left(r-r_*\right)^2 + V_0\,\theta^2$$
$$+6\,\mu\omega_*^2\left(\frac{r_*-r_\infty}{R_*}\right)\left(R-R_*\right)\left(r-r_*\right) \tag{3.9}$$

where

$$k_{saddle} = M\,\Omega^2 - 36\,\mu\omega_*^2\left(\frac{r_*-r_\infty}{R_*}\right)^2 \tag{3.10}$$

is a necessarily positive quantity. Comparison with Eq. (3.2) shows that the frequency Ω is not an observable but a zeroth-order quantity. The actual imaginary frequency at the saddle point is strongly perturbed by the curvature of the reaction path.

B. The zero initial acceleration condition

In addition to the conventional TST requirement, $P_{R^*} > 0$, additional reactivity criteria must be introduced.

The trajectory is reactive when the initial elongation δr satisfies Eq. (2.5), which becomes

$$\delta r = \left(\mu\omega_*^2\left(r_*-r_\infty\right)\right)^{-1}\left(\frac{p_\theta^2}{6\,M\,R_*^2} + V_0\,\delta\theta^2\right). \tag{3.11}$$

We note in passing that if the inter-fragment forces are assumed to decrease asymptotically as R^{-n} (i.e., if the exponent 6 that appears in Eqs. (3.4), (3.5), and (3.6) is replaced by another integer denoted n), then Eq. (3.11) remains valid with the same modification.

Deriving the expression of p_θ^2 in terms of P_{R*}^2 and of p_r^2 from the equation $H = E$ and inserting it into Eq. (3.11) leads to an alternative expression of the appropriate value to be given to δr to generate a reactive trajectory:

$$\delta r = \left(\mu \omega_*^2 \left(r_* - r_\infty\right)\right)^{-1} \left(V_0\, \delta\theta^2 + \frac{I_*}{3\mu R_*^2} \left(E - \frac{P_{R*}^2}{2M} - \frac{p_r^2}{2\mu} - V_0\, \delta\theta^2 \right) \right). \qquad (3.12)$$

C. The cubic coefficient

The leading term of the cubic coefficient c_3, whose expression for a general potential V is given by Eq. (2.6), now becomes, disregarding terms containing $\delta\theta$ and p_θ

$$c_3 = \frac{1}{M}\left(k_{saddle} \frac{P_{R*}}{M} + 6\omega_*^2 \left(\frac{r_\infty - r_*}{R_*} \right) p_r \right) + \ldots \qquad (3.13)$$

Since k_{saddle} is necessarily positive, a high value of the translational momentum P_{R*} is seen, as expected, to invariably stimulate reactivity. Furthermore, it is also found to increase the magnitude of higher odd-order coefficients.

The initial value of the vibrational momentum, p_r, also plays a role in reactivity. As shown in Eqs. (2.6) and (3.13), energy flow into the vibrational momentum is beneficial provided that the sign of p_r is properly chosen, i.e., in the present case,

$$\left(r_\infty - r_*\right) p_r > 0\,. \qquad (3.14)$$

The initial vibrational momentum p_r invariably appears in the expression of c_3, c_5, and c_7 in the form of a product $\left(r_\infty - r_*\right) p_r$. Therefore, a nonzero value of the vibrational momentum promotes reactivity only if the sign of p_r is properly coordinated with the equilibrium distances of the diatomic fragment in the TS and at its asymptotic value. Inadequate coordination curbs it.

To summarize, if the value of P_{R*} is high enough (say close to or higher than energy equipartition), then Eq. (3.11) provides in most cases a reliable way to select reactive trajectories. Together with the basic condition $P_{R*} > 0$, they provide the keys for understanding reactivity. Numerical exploratory calculations show that recrossing is then not an acute problem. The system is catapulted into the dissociation valley.

However, this is no longer the case when the value of the translational momentum is too low to provide the necessary driving force. Reactivity criteria valid for low values of P_{R*} are

then much more subtle and are one of the main issues discussed in the present paper. Essentially, reactivity is then determined by the sign of p_r because the product $\left(r_\infty - r_*\right) p_r$ must be positive, as shown in Eq. (3.14).

Two points must be clarified. First, what happens when Eq. (3.11) is not exactly fulfilled? What is the degree of tolerance? Second, a concrete appraisal of the role played by the sign and magnitude of p_r is called for.

IV. REACTIVITY LOCI IN PHASE SPACE FOR COLLINEAR TSs

To give a numerical answer to these questions, it was therefore decided to carry out a numerical study of reactivity at low values of P_{R*}.

The chosen reaction is HCO → H + CO, whose *ab initio* potential energy surface has been determined by Song *et al*.[31] The vibrational frequencies of the TS have been calculated by Cho *et al*.[32] However, two modifications were introduced to better suit the purposes of the present paper. First, the TS has been made collinear. Second, since the vibrational momentum p_r invariably appears in analytic expressions in the form of a product $\left(r_\infty - r_*\right) p_r$, it was decided to arbitrarily increase its prefactor in order to make its role more visible. Thus, r_* was assigned a value of 1.25 Å instead of the *ab initio* value of 1.153 Å. Since r_* is larger than r_∞ (which is equal to 1.128 Å), reactivity is expected to be stimulated by negative values of the initial vibrational momentum p_r.

In all of the graphics to be presented shortly, the total internal energy E has been fixed at a value of 1kcal/mol above the saddle point.

The values of the coupling parameters β_{ij} that appear in Eq. (3.8) are determined from a comparison between perturbed and unperturbed surfaces. To test issues related to separability, we want parameters that generate conspicuous distortions. The adopted surfaces are strongly but not overly distorted by the three-body interaction term.

After several exploratory calculations, it was decided to study in detail the case where the initial translational kinetic energy $P_{R*}^2 \big/ 2M$ is equal to one-tenth of that corresponding to energy equipartition, which leads to a value of the translational momentum P_{R*} equal to 0.335 a.u. (to be compared with values of 1.059 a.u. reached at equipartition, or of 2.369 a.u. when all of the internal energy flows into the translational motion). At this low value, reactivity is

essentially determined by the magnitude of the initial vibrational momentum, p_r. As expected from Eq. (3.14), all trajectories corresponding to a value of p_r whose modulus equals that corresponding to energy equipartition are found to be nicely nonrecrossing if p_r is negative, whereas none of them is reactive if p_r is strongly positive. This is easily understood: If the initial position of the representative point is larger than that of the final state, then the appropriate impulse should be given so as to bring them nearer.

A numerical illustration of the subspace of initial conditions that generate reactive trajectories can be obtained by considering active phase space graphics, constructed as follows. There are six degrees of freedom in our problem. However, the initial value of R is fixed at R_*, as it should, and the two initial momenta P_{R*} and p_r are essential parameters of the problem that determine the shape of the average equations of motion $< R(t) >$ and $< r(t) >$ and which therefore are fixed at specific values. With these prescriptions, the number of initial conditions to be specified is reduced to three.

This makes it possible to depict dynamics very descriptively via 3D-graphics, in a three-dimensional subspace ($\delta\theta$, p_θ, δr) enclosed in a parallelepiped box. The apices are fixed at the maximum possible value for these three degrees of freedom, i.e.,

$\pm(2I)^{1/2}\left(E-P_{R*}^2/2M\right)^{1/2}$ for p_θ, $\pm ArcSin\left[V_0^{-1/2}\left(E-P_{R*}^2/2M\right)^{1/2}\right]$ for $\delta\theta$, and

$\pm(2/\mu)^{1/2}\,\omega_*^{-1}\left(E-P_{R*}^2/2M\right)^{1/2}$ for δr.

To determine the influence of the initial vibrational energy, it was then decided to carry out a close examination of the neutral, unbiased case in a first set of calculations, i.e., to start with the case $p_r = 0$. The study of this case is a reference because if p_r is given a positive value, then fewer trajectories are found to be reactive, whereas if p_r is chosen to be substantially negative, then all trajectories are observed to react. The loci of initial conditions that effectively generate reactive trajectories are given in Fig. 1 as a sequence of cuts at specific values of δr.

Particular attention is paid to the subset of central reactive trajectories, i.e., the subset whose initial conditions exactly fulfill Eq. (3.11). Since $p_r = 0$, they are all expected to be reactive, as discussed in Sec.III. Their locus forms a full ellipse, represented in red in Fig.1.

The question that now arises is whether trajectories whose initial value of δr deviates somewhat from the prescription given by Eq. (3.11) will also be reactive. The answer is

positive. Unfortunately, the degree of tolerance for these adjacent trajectories (which are represented as dashed green lines in Fig. 1) cannot be predicted a priori. Furthermore, it is also observed that initial conditions that substantially depart from Eq. (3.11) may also be reactive, but at the cost of a triple recrossing of the conventional dividing surface defined by the equation $R = R_*$. The loci of this third category are represented as dotted purple segments in Fig. 1 and they delimitate the extreme initial conditions leading to reactivity. All other points of the subspace generate nonreactive trajectories, either because starting from the reactant part of the configuration space they recross at a later (positive) time, or because they describe an atom-diatom collision that fails to recombine.

Now, to illustrate the influence of the initial value of the translational momentum p_r on reactivity, similar calculations were carried out at different nonzero values of p_r. Figure 2 shows the results for the value of $p_r = +1$, to be compared with its maximum value when P_{R*} is equal to one tenth of the value corresponding to energy equipartition, which is 6.25 a.u. The reactive part of phase space is clearly substantially reduced. When $p_r = +2$, no reactive trajectory subsists and when $p_r = -2$, all of them are found to be reactive.

Comparison between Fig. 1 and Fig. 2 shows that the locus of reactive trajectories in phase space is highly specific. Altogether, only a fraction of all possible initial conditions generate truly reactive trajectories. This result had already been established by Waalkens, Burbanks, and Wiggins,[13, 33] who were able to calculate the "reactive volume", i.e., the volume of points in an energy surface corresponding to reactive trajectories. They concluded that reactive trajectories do not at all explore the energy surface ergodically and issued a warning against the use of the ergodicity assumption in statistical theories of reactivity.

V. SEPARATION OF VARIABLES IN CENTRAL REACTIVE TRAJECTORIES

We now wish to analyze in detail the behavior of the central reactive trajectories, i.e., of those whose initial value of δr satisfies Eq. (3.11), thereby reducing the magnitude of the quadratic coefficient c_2 to zero.

Consider again the first case studied in the previous section, namely that where P_{R*} is chosen to be equal to one-tenth of the value corresponding to energy equipartition, leading to a value of the translational momentum P_{R*} equal to 0.335 a.u., with $p_r = 0$, and consider the trajectories that fulfill Eq. (3.11). A representative set of ten of these central reactive

trajectories was selected at regular intervals around the red central ellipse represented in Fig. 1 and Hamilton's equations of motion were numerically integrated. The results are shown in Fig. 3 and confirm the expectations derived in Sec. II from the study of a general Hamiltonian. The ten representative trajectories are remarkably similar for the translational and vibrational spatial coordinates, but form a criss-cross of lines for the angular motion.

However, evidence for decoupling becomes spectacular when the time variable is eliminated to form a parametric plot representing the function *r(R)*. As shown in Fig. 4, the ten curves represented in red color are now undistinguishable on the scale of the graph. The explanation is clear: the slight differences between the ten trajectories observed in Fig. 3 are due to the fact that they travel at different speeds. However, they follow extremely close paths in the two-dimensional *(R, r)* configuration space, and the grouping persists during the entire reactive process, up to complete separation of fragments. By contrast, the angular motion is highly specific for each one. This establishes decoupling between angular and spatial coordinates.

Similar graphs were calculated for other values of P_{R^*} and p_r. They confirm the grouping of trajectories and hence the possibility to invoke separability of the Hamiltonian. However, although still present, the grouping is found to be less perfect when $p_r \neq 0$.

What about adjacent trajectories? Those that are still reactive deviate only slightly from the perfect grouping of the central reactive ones, as shown in Fig. 4, where two of them are represented in broken lines.

Altogether, we end up with an additional illustration of the concept of reactive cylinder (or conduit) in phase space that reactive trajectories must follow. Such conduits have been calculated by DeLeon,[26] Fair *et al*.,[27] and also, in normal form coordinates, by Wiggins,[13] Komatsuzaki,[28] and their co-workers.

VI. AN EFFECTIVE TWO-DIMENSIONAL HAMILTONIAN FOR SYMMETRICAL TSs

A. Definition

The decoupling properties established in the previous section confirm the analysis carried out in Sec. II and suggest that it should be possible to calculate the laws for the average motion along the *R* and *r* degrees of freedom by applying Hamilton's equations of

motion to a 2D Hamiltonian, thereby reducing the dimensionality of the problem. The choice of the latter is not immediately obvious, the main problem being the appropriate expression of the three-body term. If the choice is appropriate, it should generate equations of motion that coincide with those derived in Secs. III to V for the average of the central reactive trajectories.

In a heuristic approach, suggested by the fact that, as shown in Fig. 4, the actual reactive trajectories never depart very far from the reaction path and meander about it, let us define a two-dimensional Hamiltonian

$$H_{2D}\left(R,P_R,r,p_r\right)=\frac{P_R^2}{2M}+V_{saddle}\left(R\right)+\frac{P_r^2}{2\mu}+V_{diat}\left(r,R\right)+V_{3b}\left(R,r_{eq}\left(R\right),\theta_*\right). \qquad (6.1)$$

We follow the same steps as in Secs. IIC and IID and compare the coefficients from $\langle c_1\rangle$ to $\langle c_7\rangle$ and from $\langle a_1\rangle$ to $\langle a_7\rangle$, with those obtained by expanding the equations of motion in a series of nested Poisson brackets (Eqs. (2.2) and (2.3)), for the 3D and 2D Hamiltonians. As shown in the next paragraphs, it turns out that the leading terms of each coefficient are exactly the same in both cases.

B. The translational motion

First, go back to the 3D Hamiltonian defined in Eqs. (3.1) to (3.8) and used in our numerical calculations. The first term is trivial: $c_1 = P_{R*}/M$. Choosing a value of δr that fulfills Eq. (3.11) leads to $c_2 = 0$.

As already said, the observed decoupling implies that the equations of motion for the R and r degrees of freedom are independent of θ. This means that it is perfectly appropriate to concentrate on a particular solution characterized by particular initial values of $\delta\theta$ or of p_θ that simplify the calculations as much as possible. It is immediately apparent that this will be the case if we choose either of them to be equal to zero. An equivalent procedure consists of calculating an average trajectory. Then, performing the average over a set of initial conditions including positive and negative values of $\delta\theta$ and p_θ eliminates many terms. Both procedures lead to the same result. For odd-order coefficients, one finds, after getting rid of small terms,

$$\left\langle c_3\right\rangle=\frac{1}{M}\left(k_{saddle}\frac{P_{R*}}{M}+6\,\omega_*^2\left(\frac{r_\infty-r_*}{R_*}\right)p_r\right), \qquad (6.2)$$

$$\langle c_5 \rangle = \frac{\omega_*^4}{M}\left(P_{R*}\left(\left(\frac{\Omega}{\omega_*}\right)^4 + 1296\left(\frac{\mu}{M}\right)^2\left(\frac{r_\infty - r_*}{R_*}\right)^4 + 36\frac{\mu}{M}\left(\frac{r_\infty - r_*}{R_*}\right)^2\left(1-2\left(\frac{\Omega}{\omega_*}\right)^2\right)\right)\right.$$

$$\left. + 6\, p_r\left(\frac{r_* - r_\infty}{R_*}\right)\left(1 + 36\frac{\mu}{M}\left(\frac{r_* - r_\infty}{R_*}\right)^2 - \left(\frac{\Omega}{\omega_*}\right)^2\right)\right). \qquad (6.3)$$

The expression of the coefficients $< c_7 >$ is too lengthy to be reported here.

We then carried out the same expansion for H_{2D} (Eq. (6.1)). For a set of prescribed values of P_{R*} and p_r, the initial condition that remains to be specified is δr. It turns out that the choice $\delta r = 0$ generates odd-order coefficients, c_3, c_5, c_7, that exactly agree with Eqs. (6.2) and (6.3), and also with that valid for $< c_7 >$, as expected from the analysis reported in Sec. IIC. Furthermore, this choice is observed to lead also to a negligible magnitude of the first few even-order coefficients c_2 and c_4.

C. The vibrational motion

Now, consider the vibrational motion. Applying Eq. (2.2) to coordinate r leads to an expansion that can be written as

$$r(t) = r_* + a_1 t + a_2\left(\frac{t^2}{2!}\right) + a_3\left(\frac{t^3}{3!}\right) + \ldots \qquad (6.4)$$

with $a_1 = P_r/\mu$. Here again, the 3D Hamiltonian defined in Eqs. (3.1) to (3.8) and its two-dimensional approximation H_{2D} are observed to generate the same coefficients $< a_3 >$, $< a_5 >$, and $< a_7 >$ and to lead to a negligible value for $< a_2 >$ and $< a_4 >$. One gets for the leading terms

$$\langle a_3 \rangle = -\omega_*^2\left(\frac{p_r}{\mu} + 6\,\frac{P_{R*}}{M}\left(\frac{r_* - r_\infty}{R_*}\right)^2\right), \qquad (6.5)$$

$$\langle a_5 \rangle = \omega_*^4\left(1 + 36\frac{\mu}{M}\left(\frac{r_* - r_\infty}{R_*}\right)^2\right)\frac{p_r}{\mu}$$

$$+ 6\omega^2\left(\frac{r_* - r_\infty}{R_*}\right)\left(36\frac{\mu\,\omega_*^2}{M}\left(\frac{r_* - r_\infty}{R_*}\right)^2 + \left(\omega_*^2 - \Omega^2\right)\right)\frac{P_{R*}}{M}. \qquad (6.6)$$

D. Numerical calculations

High-order coefficients ($< c_9 >$, $< a_9 >$, and higher) cannot be reliably calculated analytically by this procedure because it is no longer possible to identify a main term and to neglect the remainder. The number of small terms becomes extremely large and it would be insecure to simply neglect them. Furthermore, those that should have been negligible because of the presence of several heavy nuclear masses in their denominators are now weighted by a huge numerical prefactor. However, the expansion can be carried out numerically (up to the eleventh order).

The reliability of the 2D Hamiltonian formulated in Eq. (6.1) has been checked in the case $P_{R*} = 0.335$ a.u., $p_r = 0$, and δr chosen to generate reactive trajectories. The ten central reactive trajectories studied in detail in Sec. III have been calculated by numerical integration of Hamilton's equations of motion, first by using the correct 3D Hamiltonian with δr satisfying Eq. (3.11) (exactly as in Fig. 4) and then compared with the results derived from the use of its 2D approximation (Eq. 6.1) with $\delta r = 0$. A third calculation was carried out: The equations of motion were derived using analytical formulas up to the seventh-order terms (Eqs. (6.2) to (6.6)) followed by a numerical calculation of Poisson brackets for $<c_9>$ and $<c_{11}>$. The comparison is done in Fig. 5. The green dashed line (resulting from the numerical integration of the equations of motion derived from the 2D Hamiltonian) and the red solid line (same calculations for the 3D Hamiltonian) are practically indiscernible during the entire reactive process, up to complete separation. The partially analytical calculation performs reasonably well.

VII. ADIABATICITY WITHIN THE REACTION PATH HAMILTONIAN MODEL

Various approximations have been proposed to reduce the dimensionality of a dynamical model. The physical idea underlying the vibrational adiabatic approximation is usually thought to be based on a separation of time scales. This cannot be the case here. Inspection of Fig. 3 shows that it makes little sense to try to label the three degrees of freedom as fast or slow: The relative velocities change considerably during the reaction process and the reaction is long over before the fragment can rotate by much less than 45°. In addition,

there are many indications that show that the vibrationally adiabatic approximation is valid even when the motional time scales are not appropriate.[34, 35]

In the case of an atom-diatom interaction, a number of observations can be accounted for if a specific Hamiltonian is replaced by the reaction path Hamiltonian of Miller *et al.*[36, 37] coupled with an adiabatic treatment of the bending motion.[34, 38] This model is quite compatible with the result, demonstrated in Sec. II C, that when the TS is symmetrical, the equations of motion of the average reactive trajectory can be derived from a reduced-dimensionality effective Hamiltonian, whatever the specificities of the actual three-dimensional potential energy surface.

Vibrational nonadiabaticity is known to be directly related to the curvature of the reaction path, which induces Coriolis coupling resulting from the fact that the normal mode directions wind about the reaction path.[36 – 39] As is well known, the Coriolis force deviates a trajectory either to the right or to the left, depending on the initial conditions. Therefore, in a symmetrical system, the average trajectory escapes this trend and moves in a straight line. Miller[37] has calculated the microcanonical flux through a dividing surface perpendicular to the reaction path and observes that the coupling functions no longer appear in the average flux.

What is thus the basis of an adiabatic separation leading to dimensionality reduction? It should be noted that the symmetry of the saddle point is maintained at all points along the reaction path leading from reactants through the saddle point to products.[40-42] As pointed out by Miller[42], selection rules reduce to zero Coriolis couplings between modes that belong to different irreducible representations. This is precisely the case with collinear TSs, where the bending mode decouples from the other two. Therefore, the average reactive trajectory is unaffected by Coriolis forces and the adiabatic separation holds, regardless of time scales. In short, the success of the adiabatic approximation in the reaction path Hamiltonian model is due to the symmetry of the transition state, not to a separation of time scales.

VIII. DISCUSSION

A. The strongly coordinated motion

The observed nearly perfect grouping of reactive trajectories, with negligible dispersion about the average trajectory is quite striking. A detailed analytical explanation for it is not easily found.

We put forward a model where reactive trajectories are characterized by a very strong and specific coupling between the translational and vibrational degrees of freedom, with the bending mode treated adiabatically. The term 'specific coupling' means that, as a result of the strong curvature of the reaction path, very precise motion coordination between the *R* and *r* degrees of freedom is required to usher the system into the reaction valley.

A similar description emerges from the numerous classical trajectory calculations carried out by Hutchison *et al.*[27, 43] These authors present a picture of very specific dynamics taking place in a subspace of reduced dimensionality constrained by adiabatic separation and come to the conclusion that reactivity requires "a careful phasing of a non-reactive mode with the reactive mode...". Here again, the concept of reactive cylinder in phase space that reactive trajectories must follow is recovered.

B. The Hamilton-Jacobi theory

The astonishing collimation of the reactive paths in the two-dimensional *(R, r)* configuration space is not a mere curiosity. The Hamilton-Jacobi formalism tells us that we come here to a fundamental point. This theory holds that, if the Hamiltonian is time-independent, at any point **r** of the configuration space, the momentum **P** of a trajectory is given by the gradient of the so-called characteristic function W (defined as $W = \int \sum_i p_i \, dq_i$).[25]

Thus, the equation W = constant represents a set of surfaces in configuration space and the equation

$$\mathbf{P}(\mathbf{r}) = \mathbf{grad}(W(\mathbf{r})) \qquad (8.1)$$

means that the flow of reactive trajectories is orthogonal to the surfaces of constant action. It follows that if the paths of the subset of reactive trajectories are identical, then the function W is locally planar.

The above picture of a family of surfaces of constant action pierced by a family of perpendicular lines that are the particle trajectories makes it possible to describe mechanical motions in terms similar to those used in optics, where waves propagate with a wave vector locally perpendicular to the wave front.[44, 45] However, the analogy extends only to the paths of mechanical particles and does not include the manner in which the motion occurs in time. Therefore, time has to be eliminated from relevant trajectory calculations and replaced by *R* as the appropriate independent variable. This is done in Fig. 6, which shows, for each of the ten central reactive trajectories represented in Figs. 3, 4, and 5, the three momenta P_R, P_r, and P_θ,

plotted as a function of R. The decoupling is obvious. Clearly, the ten reactive trajectories have extremely close (although not strictly identical) translational momenta P_R. The same is true for the vibrational momenta P_r. By contrast, each initial value of the angular momentum initiates a specific $P_\theta(R)$ trajectory. In other words, all of the central reactive trajectories are characterized by nearly identical projections of the momentum vector **P** on the *(R, r)* plane during the entire evolution.

The characteristic function W depends on the spatial variables (i.e., in the present case, the three coordinates R, r, and θ) and also on a set of constants related to the initial conditions. The interpretation to be given the grouping observed in Fig. 6 is that when these initial conditions are chosen to generate reactive trajectories, the characteristic function is locally planar over that part of configuration space corresponding to the subspace that is covered by central reactive trajectories. As one considers adjacent trajectories, the different curves $P_R(R)$ and $P_r(R)$ exhibit dispersion (as can be seen in Fig. 4), which means that deviations from planarity become conspicuous.

Since, despite the nonseparability of the characteristic function, attention can be focused on a 2D system confined to the (R, r) space, and since reactive trajectories starting at two points separated by an infinitesimal distance obviously remain practically undistinguishable, it can be said that the Liapunov exponent of reactive trajectories is zero. The collimation of the trajectories observed by Berry and his co-workers in the isomerization of argon complexes[9-12] provides possibly an additional example.

Note finally that this analysis is based on numerical evidence. One can only note the tightness of the grouping without being able to identify its deep-seated reasons.

IX. HIGHER ENERGY

We now consider the effect of an increase in the total energy E. At high internal energies, the locus of central reactive trajectories no longer forms a complete ellipse, but splits into a pair of reactive segments, as shown in Fig. 7, which deals with the case $E = 10$ kcal/mol. The region in phase space that generates reactive trajectory decreases as energy increases, as shown by comparison between Figs. 1 and 7. So does the transmission coefficient, in conformity with an argument already put forward by Hirschfelder and Wigner[2].

As shown in Fig. 8, the grouping of the central reactive trajectories persists, although a slight dispersion is now conspicuous. The two-dimensional approximation is quite

satisfactory, up to complete separation. Separability and dimensionality reduction thus remain valid at higher energies.

X. BENT TRANSITION STATES

To check whether decoupling is an inherent characteristic of reactive trajectories and not the result of the fact that considerations have been restricted to collinear TSs, the case of a T-shaped TS has been briefly studied.

To achieve C_{2v} symmetry, we consider the fictitious reaction $HN_2 \rightarrow H + N_2$, with $\theta_* = \pi/2$, making otherwise as few adjustments as possible to the previous model. The total internal energy E has again been fixed at a value of 1kcal/mol above the saddle point.

As shown in Fig. 9, the locus of central reactive trajectories no longer forms a full circle, but takes a more complicated shape. However, the features demonstrating dynamic regularity subsist. As seen in Fig. 10, the grouping of the central reactive trajectories persists, although a slight dispersion is now visible. The two-dimensional Hamiltonian H_{2D} (dashed line) performs remarkably well during the entire lifetime of the reaction.

XI. CONCLUDING REMARKS

The most important finding of this work is the close connection between reactivity, separability, and dimensionality reduction, which has been well established for symmetrical TSs. Simply put, separability and dynamic regularity are specific characteristics of reactive trajectories.

The present procedure (which is limited to a triatomic system only) is based on the specificities of central reactive trajectories, which have been shown to display intrinsic characteristics such as grouping (which might also be termed collimation[9-12] and which implies zero Liapunov coefficients), dimensionality reduction, ray property, local planarity of the Hamilton characteristic function, and which persist for the entire duration of the reaction, as the figures illustrate.

However, the picture that emerges from the present work differs from that established by Wiggins, Berry, Komatsuzaki, and their co-workers.[12-15, 28] In the approach of these authors, the coordinate transformation leads to a separation into n decoupled systems that fully satisfies chemists: an unstable degree of freedom and $n–1$ bath oscillators. This result establishes a framework of fundamental importance. However, it may lose its appeal when

transformed back into the original coordinate system. Here, we end up with an unexpected result involving strong coordination between two degrees of freedom, whereas the third one is separable because it belongs to a different irreducible representation.

In the search for reactivity criteria, what we really end up with is a set of propensities, unfortunately insufficient to exactly delimitate the active part of phase space. The main additional criterion introduced in this study is the zero initial acceleration condition $c_2 = 0$, which is necessary to counteract the curvature of the reaction path, and which finds its analytical expression in Eqs. (2.5), (3.11), and (3.12). It means that a trajectory will be reactive only if it properly makes the initial turn in configuration space imposed by the curvature of the reaction path. However, surprisingly effective as it is, this new reactivity criterion is not sufficient: the condition $c_3 > 0$, leading to Eqs. (2.7) or (3.14), also plays a role, at least at low values of P_{R^*}. Nor is it necessary: sufficiently close adjacent initial conditions also generate reactive trajectories. Nevertheless, these equations identify what can be termed the hard core of reactive trajectories.

Our analysis has been carried out under the assumption of a symmetrical TS. Unsymmetrical ones present a problem because of the difficulty of finding a set of four equivalent initial positions having the same energy. Considering microcanonical averages with a finite energy width might solve the problem, but we leave this for possible future work.

What is particularly surprising is that, although Eqs. (2.5) or (3.11) plus (2.7) or (3.14) are highly local initial conditions which in principle can only provide a good start, they are observed to generate a tightly-packed bundle that maintains its extraordinarily coherent motion in the two-dimensional *(R, r)* configuration space, during the entire reactive process, up to complete separation of fragments, as shown in Figs. 3, 4, and 6. An in-depth explanation is clearly called for.

Since it has been demonstrated in Sec. II that the dimensionality reduction is not directly linked to characteristics of the potential energy surface, its effective success, demonstrated in Figs. 5, 8, and 10, shows that the basic reasons can be found in symmetry considerations (which reduce to zero the Coriolis couplings for the average reactive trajectory), rather than in, e.g., the smallness of mode-mode couplings. Neither should it be sought in a separation of time scales.

Finally, an essential point that emerges is the specific behavior of reactive trajectories which, as already noted by Wiggins and co-workers,[13, 25] do not behave ergodically. Only a small fraction of possible initial conditions generate reactive trajectories and their localization in phase space is not at all random, as shown by Figs. 1, 2, 7, and 9. This raises serious

questions about the validity of statistical methods since decoupling prevents rapid and extensive energy redistribution between modes. However, it is difficult to be more specific at this juncture, because any discussion of the assumption of ergodicity on which TST is based must beforehand specify the way (thermal or specific) energy is delivered to the molecule.[46-49] This issue has not been addressed here.

ACKNOWLEDGMENT

It is a pleasure to thank Professor Bernard Leyh for helpful discussions and comments.

REFERENCES

[1]W. H. Miller, Acc. Chem. Res. **9**, 306 (1976).

[2]J.O. Hirschfelder and E. Wigner, J. Chem. Phys. **7**, 616 (1939).

[3]R.A. Marcus, J. Chem. Phys. **45**, 4500 (1966).

[4]R. A. Marcus, Science **256**, 1523 (1992).

[5]D. G. Truhlar, J. Chem. Phys. **53**, 2041 (1970).

[6]W. H. Miller, Faraday Discuss. Chem. Soc. **62**, 40 (1977).

[7]S. Keshavamurthy and W. H. Miller, Chem. Phys. Lett. **205**, 96 (1993).

[8]R. Hernandez and W. H. Miller, Chem. Phys. Lett. **214**, 129 (1993).

[9]D. J. Wales and R. S. Berry, J. Phys. B **24**, L351 (1991).

[10]R. J. Hinde, R. S. Berry and D. J. Wales, J. Chem. Phys. **96**, 1376 (1992).

[11]R. J. Hinde and R. S. Berry, J. Chem. Phys. **99**, 2942 (1993).

[12]T. Komatsuzaki and R. S. Berry, J. Chem. Phys. **110**, 9160 (1999).

[13]H. Waalkens, A. Burbanks and S. Wiggins, J. Chem. Phys. **121**, 6207 (2004).

[14]H. Waalkens, R. Schubert and S. Wiggins, Nonlinearity **21**, R1 (2008).

[15]A. Goussev, R. Schubert, H. Waalkens and S. Wiggins, Adv. Quantum Chem. **60**, 269 (2010).

[16]J. C. Lorquet, J. Chem. Phys. **140**, 134303 (2014), erratum: **140**, 169902 (2014).

[17]J. C. Lorquet, J. Chem. Phys. **140**, 134304 (2014).

[18]J. C. Lorquet, J. Chem. Phys. **143**, 104314 (2015).

[19]J. O. Hirschfelder, Int J. Quantum Chem. **3** (S3a), 17 (1969).

[20](a) L.P. Sun, K. Y. Song, and W. L. Hase, Science **296**, 875 (2002); (b) J. G. Lopez, G. Vayner, U. Lourderaj, S. V. Addepalli, S. Kato, W. A. deJong, T. L. Windus, and W. L. Hase, J. Am. Chem. Soc. **129**, 9976 (2007).

[21]B. Lasorne, G. Dive, D. Lauvergnat and M. Desouter-Lecomte, J. Chem. Phys. **118**, 5831 (2003).

[22]P. Collins, B. K. Carpenter, G. S. Ezra and S. Wiggins, J. Chem. Phys. **139**, 154108 (2013).

[23]J. M. Bowman and B. C. Shepler, Annu. Rev. Phys. Chem. **62**, 531 (2011).

[24]F. A. L. Mauguière, P. Collins, G. S. Ezra, S. C. Farantos and S. Wiggins, J. Chem. Phys. **140**, 134112 (2014).

[25]H. Goldstein, C. Poole and J. Safko, *Classical Mechanics*. (Addison Wesley, San Francisco, 2002).

[26]N. DeLeon, J. Chem. Phys. **96**, 285 (1992).

[27]J. R. Fair, K. R. Wright and J. S. Hutchinson, J. Phys. Chem. **99**, 14707 (1995).

[28]C. B. Li, Y. Matsunaga, M. Toda and T. Komatsuzaki, J. Chem. Phys. **123**, 184301 (2005).

[29]G. Simons, R. G. Parr and J. M. Finlan, J. Chem. Phys. **59**, 3229 (1973).

[30]J. N. Murrell, S. Carter, S. C. Farandos, P. Huxley and A. J. C. Varandas, *Molecular Potential Energy Functions* (Wiley, Chichester, 1984).

[31]L. Song, A. van der Avoird and G. Groenenboom, J. Phys. Chem. A **117**, 7571 (2013).

[32]S. W. Cho, W. L. Hase and K. N. Swamy, J. Phys. Chem. **94**, 7371 (1990).

[33]H. Waalkens, A. Burbanks and S. Wiggins, Phys. Rev. Lett. **95**, 084301 (2005).

[34]J.M. Bowman, Adv. Chem. Phys. **65**, 61 (1985).

[35]G. C. Schatz, J. Chem. Phys. **79**, 5386 (1983).

[36]W. H. Miller, N. C. Handy, and J. E. Adams, J. Chem. Phys. **71**, 99 (1980).

[37]W. H. Miller, J. Phys. Chem. **87**, 3811 (1983).

[38]R.T. Skodje and D. G. Truhlar, J. Chem. Phys. **79**, 4882 (1983).

[39]G. L. Hofacker and R. D. Levine, Chem. Phys. Lett. **9**, 617 (1971).

[40]R. G. Pearson, Acc. Chem. Res. **4**, 152 (1971).

[41]P. Pechukas, in *Dynamics of Molecular Collisions. PartB*, edited by W. H. Miller (Plenum, New York, 1976), pp. 269–322.

[42]W. H. Miller, J. Am. Chem. Soc. **105**, 216 (1983).

[43]J. S. Hutchinson, in *Dynamics of Molecules and Chemical Reactions*, edited by R. E. Wyatt and J. Z. H. Zhang (Marcel Dekker, New York, 1996), Chap. 14.

[44]R.C. Tolman, *The Principles of Statistical Mechanics* (Oxford University Press, London,1936).

[45]C. Lanczos, *The Variational Principles of Mechanics* (University of Toronto Press, Toronto, 1970).

[46]U. Lourderaj and W. L. Hase, J. Phys. Chem. A **113**, 2236 (2009).

[47]S. Yu. Grebenshchikov, R. Schinke, and W. L. Hase, in *Unimolecular Kinetics: Part 1. The Reaction Step*, Comprehensive Chemical Kinetics Vol. 39, edited by N. J. B. Green (Elsevier, New York, 2003), pp. 105–242.

[48]W. L. Hase and R. Schinke, in *Theory and Applications of Computational Chemistry: The First Forty Years*, edited by C. Dykstra, G. Frenking, K. S. Kim, and G. E. Scuseria (Elsevier, New York, 2005), pp. 397–423.

[49]G. S. Ezra, H. Waalkens, and S. Wiggins, J. Chem. Phys. **130**, 164118 (2009).

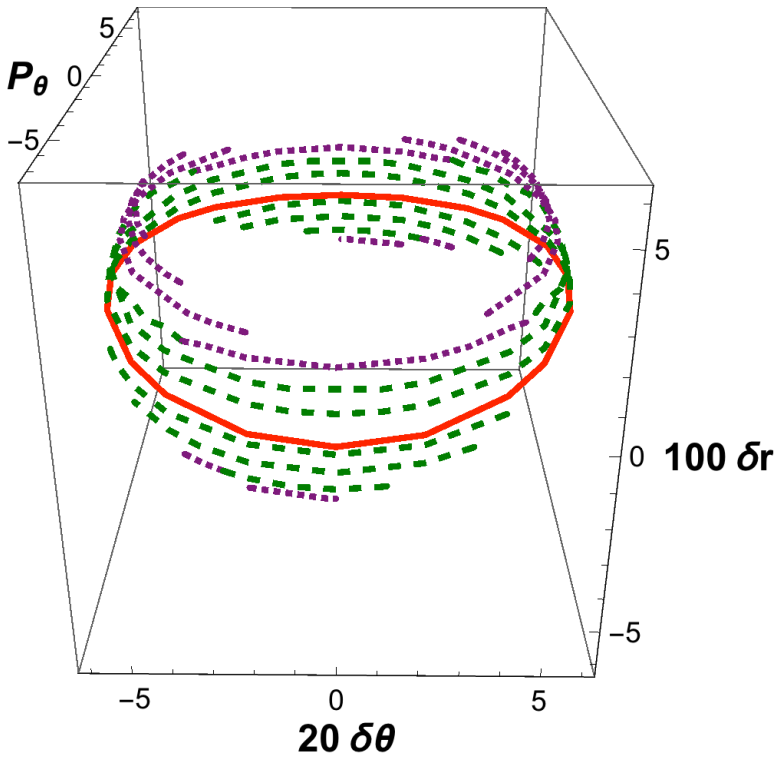

FIG. 1. Active phase space graphic for a low value of P_{R^*} (i.e., $P_{R_*}^2 \big/ 2M = E/50$) (with E = 1kcal/mol) and for $p_r = 0$. Atomic units are used throughout. Red solid line: locus of initial conditions satisfying Eq. (3.11) and generating central reactive trajectories. Dashed green lines: loci of initial conditions generating adjacent reactive trajectories. Dotted purple lines: loci generating triply recrossing trajectories.

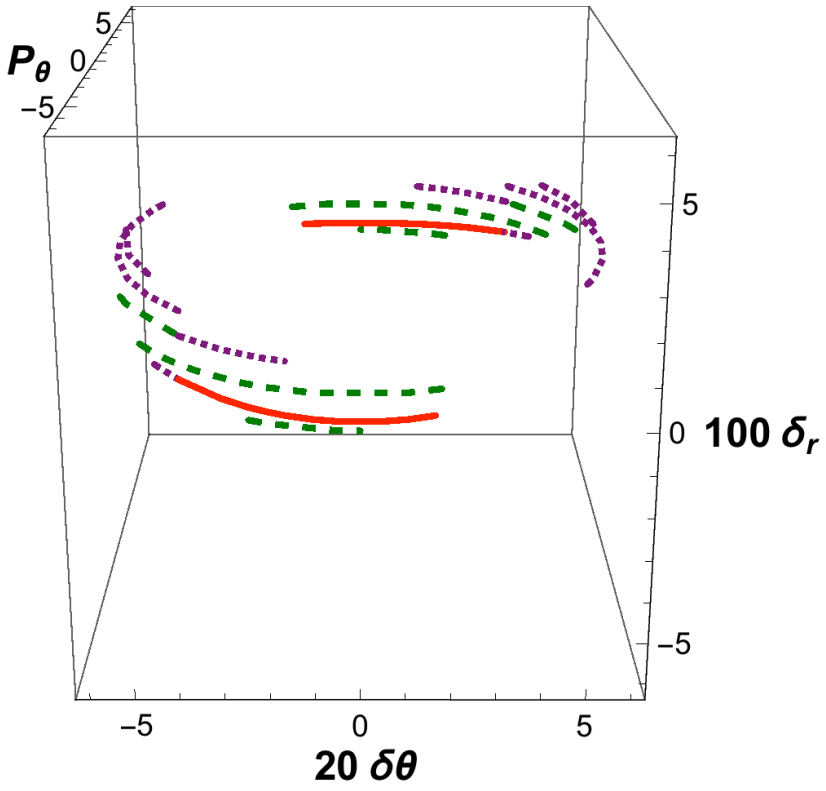

FIG. 2. Active phase space graphic for a low value of P_{R*} (i.e., $P_{R*}^2 \big/ 2M = E/50$) (with E = 1kcal/mol) and for $p_r = +1$, showing the adverse influence on reactivity due to a positive value of p_r. Atomic units are used throughout. Red solid line: locus of initial conditions satisfying Eq. (3.11) and generating central reactive trajectories. Dashed green lines: loci of initial conditions generating adjacent reactive trajectories. Dotted purple lines: loci generating triply recrossing trajectories.

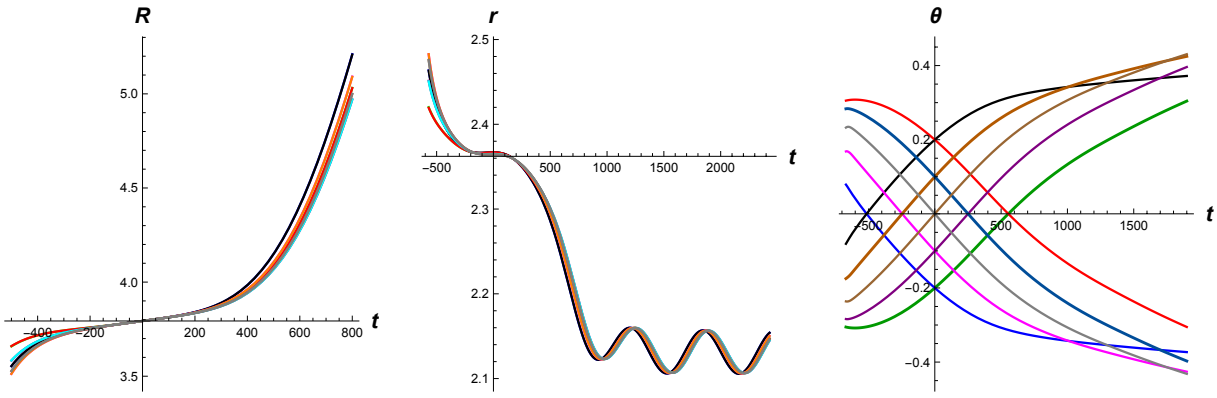

FIG.3. Graphs showing ten individual central reactive trajectories, calculated for a low value of P_{R*} (i.e., $P_{R*}^2 \big/ 2M = E/50$) (with E = 1kcal/mol) and for $p_r = 0$. Atomic units are used throughout.

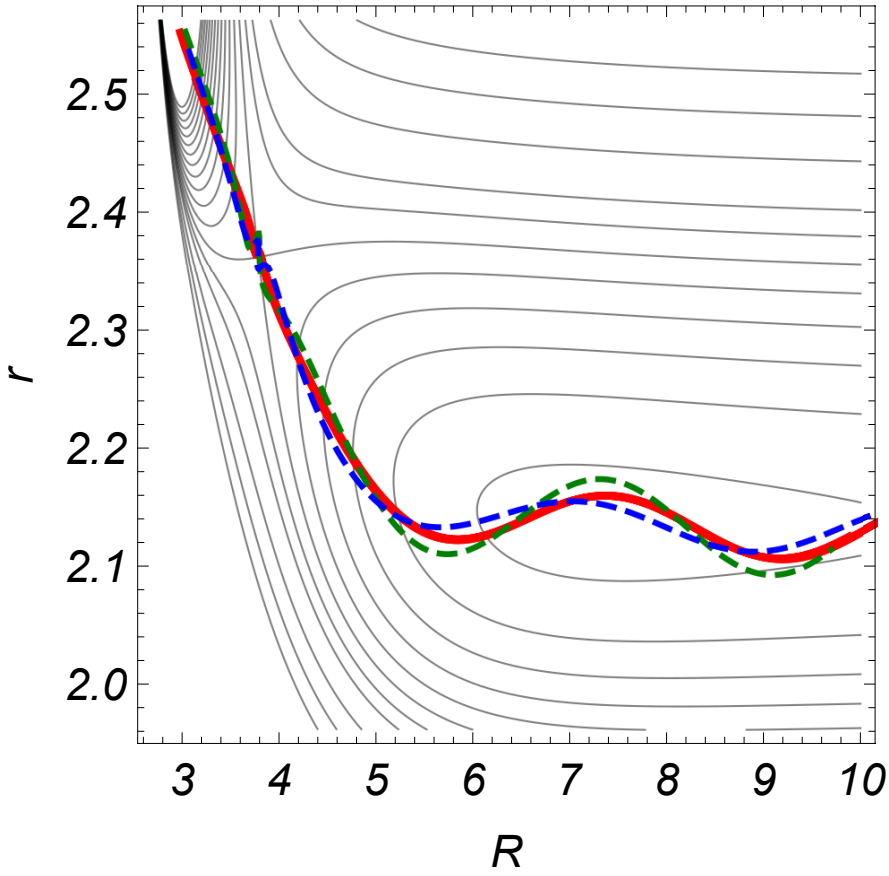

FIG. 4. Reactive trajectories projected on the contour diagram of the potential energy surface of a collinear TS when $P_{R*}^2 / 2M = E/50$ (with E = 1 kcal/mol) and $p_r = 0$. Atomic units are used throughout. The red solid line results from the superposition of the ten central reactive trajectories depicted in Fig. 3. The two dashed lines represent two typical adjacent trajectories arbitrarily chosen on the green loci of Fig. 1.

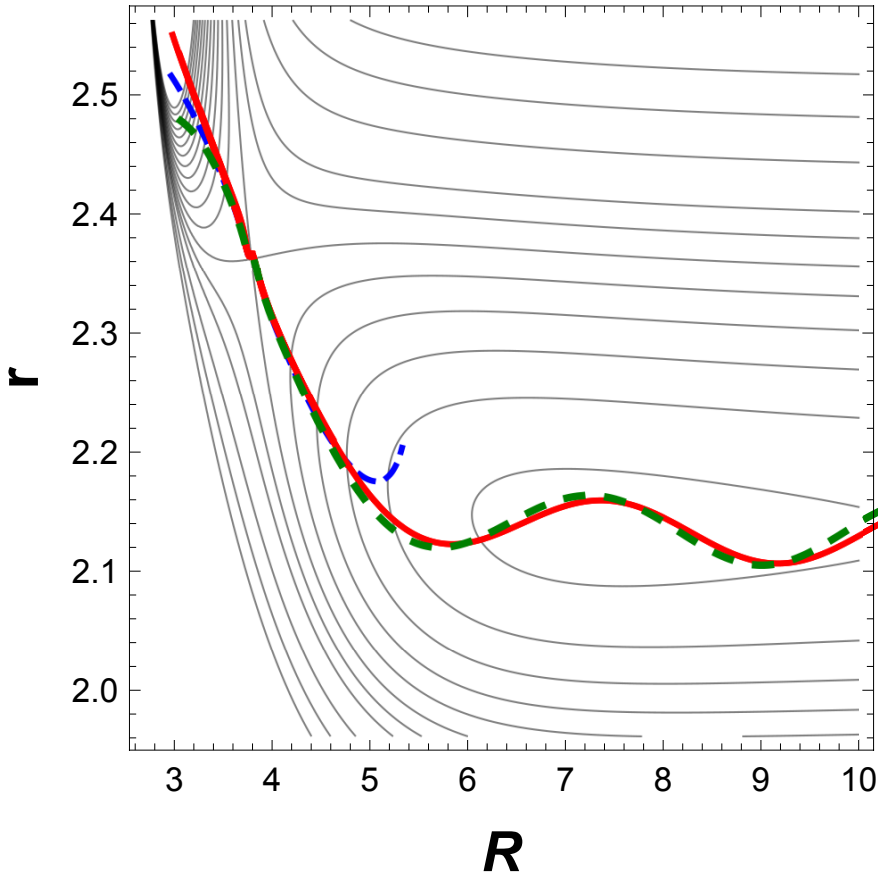

FIG.5. Reactive trajectories projected on the contour diagram of the potential energy surface of a collinear TS when $P_{R*}^2 \big/ 2M = E/50$ (with E = 1 kcal/mol) and $p_r = 0$. Atomic units are used throughout. The red solid line results from the superposition of the ten central reactive trajectories depicted in Fig. 3. The green dashed line, which results from a similar calculation carried out with the 2D Hamiltonian (Eq. (6.1)), is seen to perform remarkably well up to complete separation of the fragments. The blue dashed line results from an analytical (up to the seventh order), then numerical (up to the eleventh order) expansion in Poisson brackets of the equations of motion (Eqs. (2.9) and (2.10)).

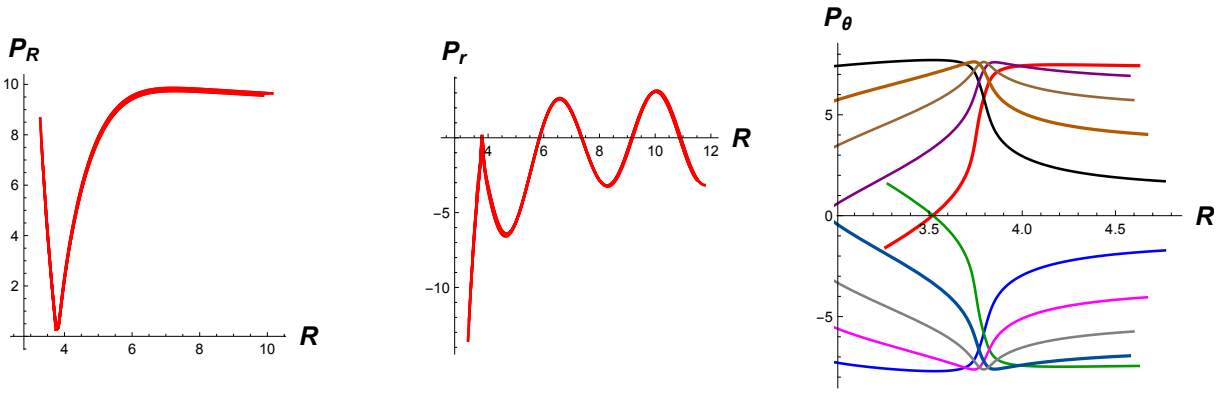

FIG. 6. Graphs showing the evolution of the three momenta of a collinear TS as a function of the translational coordinate R, for ten individual central reactive trajectories, calculated at a low value of P_{R*} (i.e., $P_{R*}^2 \big/ 2M = E/50$), with E = 1kcal/mol, and with $p_r = 0$. Atomic units are used throughout.

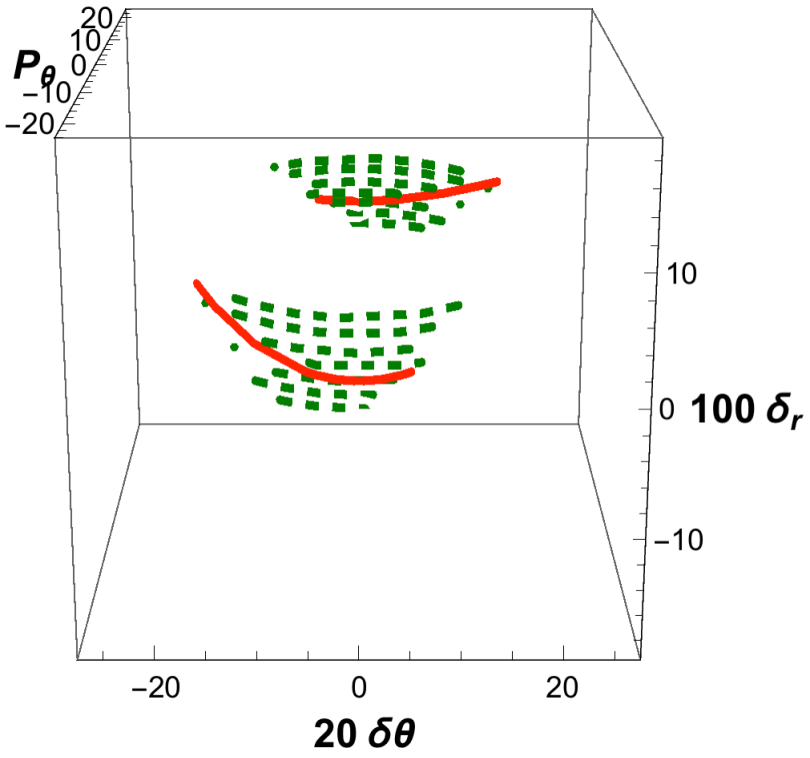

FIG. 7. The high-energy case (E = 10 kcal/mol): Active phase space graphic for a collinear TS studied at a low value of P_{R*} (i.e., $P_{R*}^2 \big/ 2M = E/50$) and for $p_r = 0$. Atomic units are used throughout. Red solid line: locus of initial conditions satisfying Eq. (3.11) and generating central reactive trajectories. Dashed green lines: loci of initial conditions generating adjacent reactive trajectories.

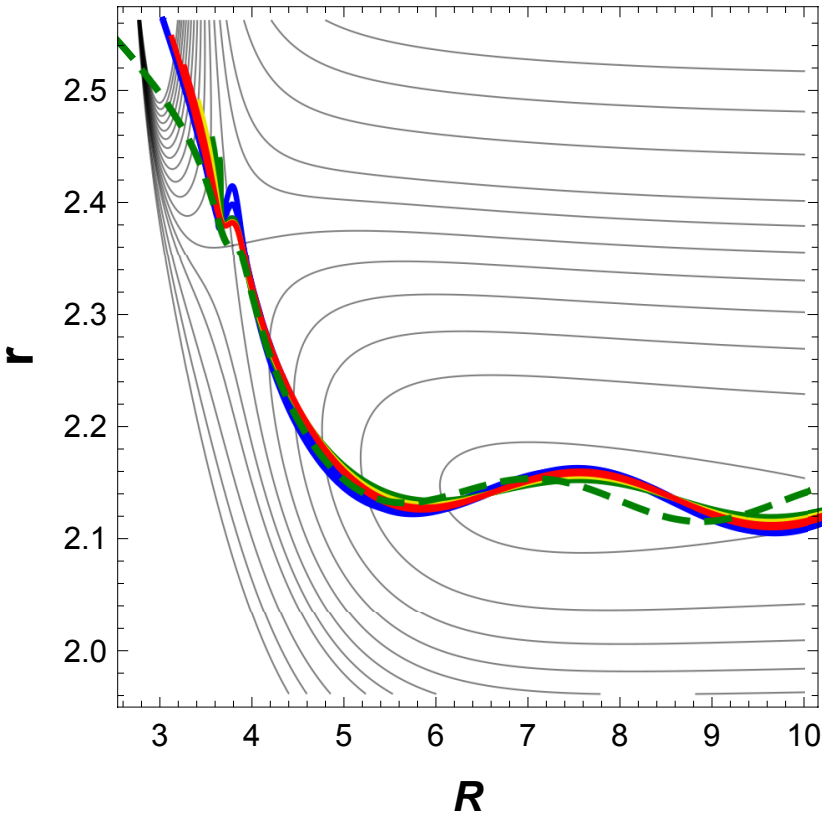

FIG. 8. The high-energy case (E = 10 kcal/mol): Reactive trajectories projected on the contour diagram of the potential energy surface of a collinear TS when $P_{R*}^2 \big/ 2M = E/50$ and $p_r = 0$. Atomic units are used throughout. Nine central reactive trajectories are represented in different colors, to show a slight, but conspicuous, dispersion. The green dashed line, which results from a similar calculation carried out with the 2D Hamiltonian (Eq. (6.1)), provides a satisfactory approximation.

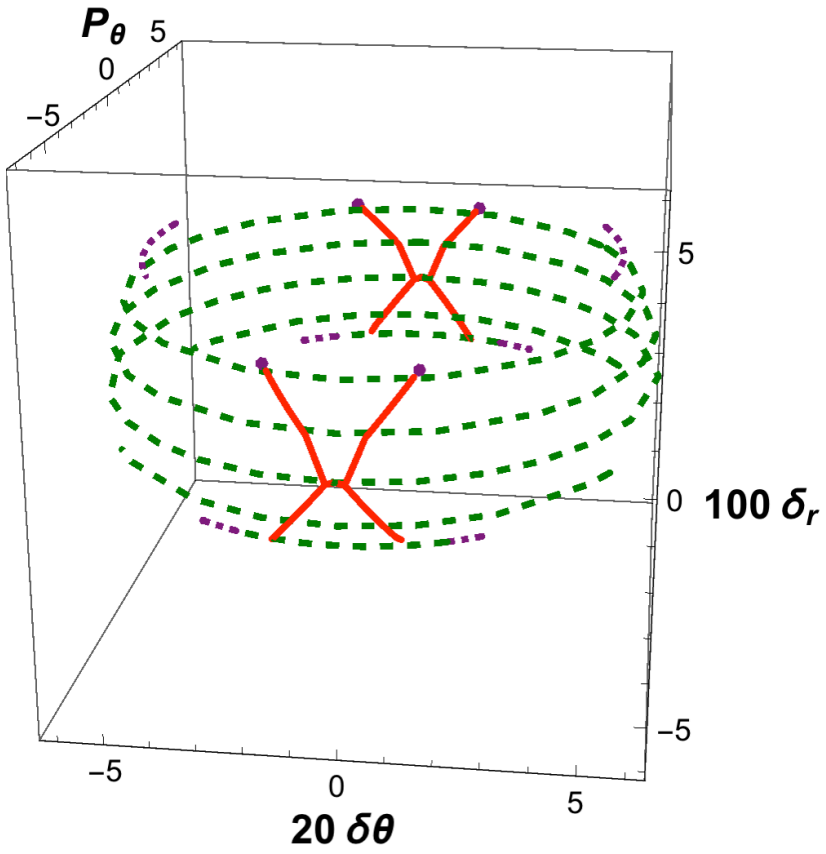

FIG. 9. The T-shaped case: Active phase space graphic for a C_{2v} TS studied at a low value of P_{R*} (i.e., $P_{R*}^2 \big/ 2M = E/50$) (with E = 1 kcal/mol) and for p_r = 0. Atomic units are used throughout. Red solid line: locus of initial conditions satisfying Eq. (3.11) and generating central reactive trajectories. Dashed green lines: loci of initial conditions generating adjacent reactive trajectories. Dotted purple lines: loci generating triply recrossing trajectories.

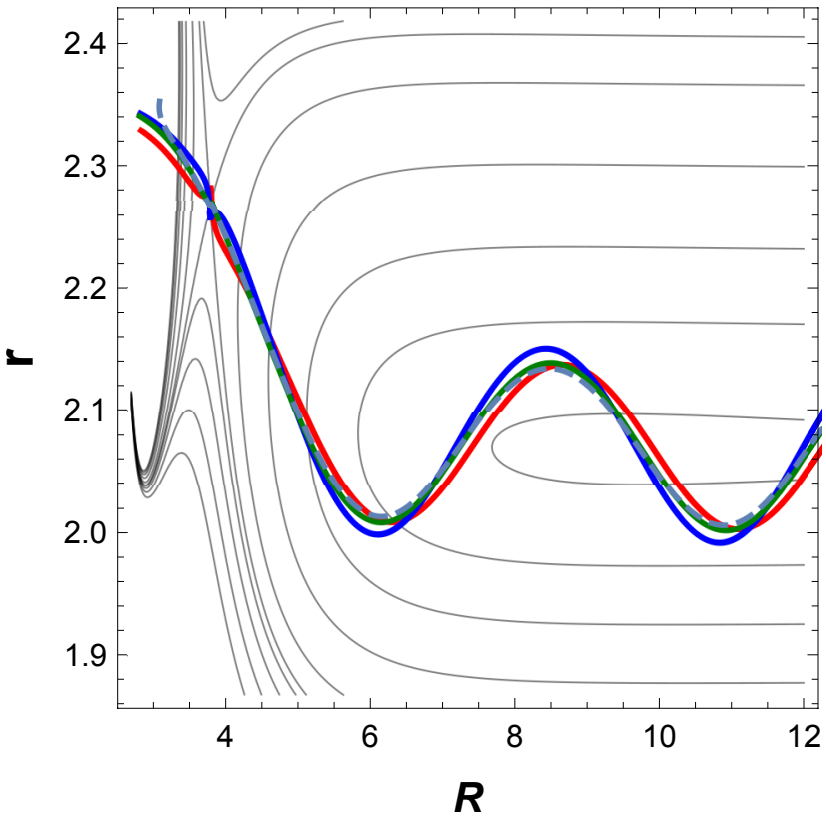

FIG. 10: Reactive trajectories projected on the contour diagram of the potential energy surface of a T-shaped TS when $P_{R*}^2 / 2M = E/50$ (with E = 1 kcal/mol) and $p_r = 0$. Atomic units are used throughout. The solid lines result from the superposition of five central reactive trajectories. The green dashed line, which results from a similar calculation carried out with the 2D Hamiltonian (Eq. (6.1)), performs remarkably well up to complete separation of the fragments.